




# Geophysical Research Letters®



## RESEARCH LETTER

10.1029/2024GL114425

## Electron Beams Generated by the Electron Kelvin-Helmholtz Instability at a Quasi-Perpendicular Shock

Ao Guo<sup>1,2,3</sup> , Quanming Lu<sup>1,2,3</sup> , San Lu<sup>1,2,3</sup> , Xinliang Gao<sup>1,2,3</sup>, and Zhongwei Yang<sup>4</sup>

<sup>1</sup>CAS Key Lab of Geospace Environment, School of Earth and Space Sciences, University of Science and Technology of China, Hefei, China, <sup>2</sup>CAS Center for Excellence in Comparative Planetology, Hefei, China, <sup>3</sup>Collaborative Innovation Center of Astronautical Science and Technology, Harbin, China, <sup>4</sup>State Key Laboratory of Solar Activity and Space Weather, National Space Science Center, Chinese Academy of Sciences, Beijing, China

### Key Points:

- For the first time, we reveal that the electron Kelvin-Helmholtz instability can be excited at the ramp of quasi-perpendicular shocks
- The parallel electric field is formed in the electron vortices generated by the electron Kelvin-Helmholtz instability
- Electrons can be trapped in the vortices and accelerated by the parallel electric field, leading to the formation of field-aligned beams

### Supporting Information:

Supporting Information may be found in the online version of this article.

### Correspondence to:

Q. Lu,  
[qmlu@ustc.edu.cn](mailto:qmlu@ustc.edu.cn)

### Citation:

Guo, A., Lu, Q., Lu, S., Gao, X., & Yang, Z. (2025). Electron beams generated by the electron Kelvin-Helmholtz instability at a quasi-perpendicular shock. *Geophysical Research Letters*, 52, e2024GL114425. <https://doi.org/10.1029/2024GL114425>

Received 3 JAN 2025  
Accepted 24 FEB 2025

**Abstract** Electron beams are considered to be important free energy sources for the excitation of various plasma waves at quasi-perpendicular shocks. In this article, we perform a two-dimensional particle-in-cell simulation of a low-plasma- $\beta$  quasi-perpendicular shock. The magnetic field at the shock ramp has a large gradient, where upstream electrons and ions are separated due to their different gyro-radius. This charge separation induces a sub-ion scale electric field at the shock ramp. The electric drift of electrons in this field can induce an electron shear flow, resulting in the excitation of Kelvin-Helmholtz instability and the generation of electron vortices. These vortices further cause charge separation at their centers, resulting in a large electrostatic field. The electrons trapped in these vortices can gain energy from the parallel component of the electric field, which eventually leads to field-aligned electron beams. Our results provide a novel process for generating electron beams at low-plasma- $\beta$  quasi-perpendicular shocks.

**Plain Language Summary** Satellite observations suggest that electron beams are vital components at quasi-perpendicular shocks, but their formation mechanism in low- $\beta$  plasma remains unclear. Using advanced numerical simulations, we investigated how these electron beams are formed. We discovered that at the shock front, ions can penetrate deeper into the shock ramp than the electrons because of their larger gyro-radius, which causes charge separation and induces a sub-ion scale electric field. The electric drift of electrons in this field can further lead to the emergence of vortices due to the electron Kelvin-Helmholtz instability. Electrons trapped in these vortices can be accelerated in the direction parallel to the magnetic field. Field-aligned electron beams are then formed. Our findings can provide new insights into how electron beams are formed in low-plasma- $\beta$  environments.

## 1. Introduction

Collisionless shock waves ubiquitously exist in space and astrophysical plasma, which can be separated into two categories according to the angle between the upstream magnetic field and the shock normal ( $\theta_{Bn}$ ) (Bale et al., 2005; Balogh & Treumann, 2013; Burgess et al., 2005): quasi-parallel shocks ( $\theta_{Bn} < 45^\circ$ ) and quasi-perpendicular shocks ( $\theta_{Bn} > 45^\circ$ ). In the solar system, quasi-perpendicular shocks have been extensively studied through in situ observations (Balogh & Treumann, 2013; Stone & Tsurutani, 1985; Tsurutani & Stone, 1985). Plasma waves are commonly detected by spacecraft at these quasi-perpendicular shocks, such as Langmuir waves and electrostatic waves, which are believed to be excited by field-aligned electron beams (Bale et al., 1999; Gurnett et al., 1979; Pulupa et al., 2010; Williams et al., 2005). Moreover, the occurrence of type II solar radio bursts is also related to field-aligned electron beams at quasi-perpendicular shocks driven by coronal mass ejections (CMEs) (Bale et al., 1999; Holman & Pesses, 1983; Jebaraj et al., 2021; Maloney & Gallagher, 2011; Melrose, 1980, 2017; Morosan et al., 2019). Recently, with high-resolution satellite measurements, field-aligned electron beams have been directly observed at quasi-perpendicular shocks (Lindberg et al., 2023; Wilson et al., 2016). These beam electrons may be further scattered upstream and downstream by plasma waves and eventually accelerated to high energy (Bell, 1978; Drury, 1983).

Shock drift acceleration (SDA) has been regarded as the primary mechanism for generating electron beams at quasi-perpendicular shocks (Amano et al., 2022; Wu, 1984). In SDA, part of the upstream electrons is reflected by the shock and gain energy through their gradient drift anti-parallel to the upstream motional electric field ( $\mathbf{E}_{\text{motional}} = -\mathbf{V} \times \mathbf{B}$ ). However, a large number of shocks in the solar system occur in low-plasma- $\beta$  environments, such as the CME-driven shocks (Bale et al., 2016; Maguire et al., 2020; Maloney & Gallagher, 2011;

© 2025. The Author(s).

This is an open access article under the terms of the [Creative Commons Attribution License](https://creativecommons.org/licenses/by/4.0/), which permits use, distribution and reproduction in any medium, provided the original work is properly cited.

Morosan et al., 2019; Shen et al., 2022). Thermal electrons can hardly be directly accelerated by SDA in low-plasma- $\beta$  environments (Holman & Pesses, 1983; Jebaraj et al., 2021), which makes the generation of electron beams inexplicable. In this article, we present a novel process for generating electron beams at a low-plasma- $\beta$  quasi-perpendicular shock using a two-dimensional (2D) particle-in-cell (PIC) simulation. For the first time, we find that the electron Kelvin-Helmholtz instability (EKHI) can be excited by the electron shear flow at the shock ramp. Electron vortices are formed by this instability and cause charge separation at their centers. Thermal electrons can be directly accelerated by the parallel component of the electric field while drifting together with the vortices. These accelerated electrons eventually form field-aligned beams at the shock ramp.

## 2. Simulation Model

We use an open-source electromagnetic PIC code called Smilei (Derouillat et al., 2018) to investigate quasi-perpendicular shocks. The simulation is carried out in the  $x - y$  plane. The size of the simulation domain is  $L_x \times L_y = 122.88d_{i0} \times 10.24d_{i0}$ , where  $d_{i0} = \frac{c}{\omega_{pi0}}$  is the ion inertial length. Periodic condition is applied in the  $y$  direction. To create the shock, we employ the injection method (Matsukiyo & Scholer, 2012). Particles are continuously injected from the left boundary ( $x = 0$ ) with a bulk velocity in  $+x$  direction ( $V_{in} = 3V_{A0}$ , where  $V_{A0}$  is the Alfvén speed), and are specularly reflected at the right boundary ( $x = L_x$ ). The formation of the quasi-perpendicular shock is mediated by a modified two-stream instability (MTSI) between the injected and reflected ions, which makes the formation time much less than an ion gyro-period ( $T_{ci} = \frac{2\pi}{\Omega_{i0}}$ , where  $\Omega_{i0} = \frac{eB_0}{m_i}$  is the ion gyro-frequency) (Zhang et al., 2021, 2024). The shock moves in  $-x$  direction after its formation. The upstream magnetic field is set with an out-of-plane component:  $\mathbf{B}_0 = (B_0 \cos \theta_{Bn}, 0, B_0 \sin \theta_{Bn})$ , where  $\theta_{Bn} = 85^\circ$  is the shock normal angle. We adopt the ion-to-electron mass ratio of  $m_i/m_e = 100$ , the upstream plasma  $\beta_i = 0.1$ ,  $\beta_e = 0.2$ , and the light speed  $c = 50V_{A0}$ . The size of the computational cell is  $d_x = d_y = 0.01d_{i0}$ , and each cell contains 80 computational particles initially. The simulation is pushed at a timestep of  $\Omega_{i0}\Delta t = 1 \times 10^{-4}$ .

## 3. Results

The shock propagates leftward with a speed of about  $1.8V_{A0}$  after it is detached from the right boundary, which means the Alfvén Mach number ( $M_A$ ) is about 4.8 in the shock rest frame. The simulation parameters ( $M_A \approx 4.8, \beta_e = 0.2$ ) are typical for shocks in the solar corona and the near-sun solar wind. Movies S1 and S2 show the evolution of the nonstationary shock structure from  $\Omega_{i0}t = 10.0$  to 17.0, where a periodic reappearance of a new shock front ahead of the shock can be observed. This is the typical reformation process of quasi-perpendicular shocks (Biskamp & Welter, 1972; Lembège & Dawson, 1987; Lembège & Savoini, 2002; Yang et al., 2020). According to Hellinger et al. (2002), the parameters used in our simulation also meet the conditions for shock reformation. The fully developed shock structure at  $\Omega_{i0}t = 16.6$  is illustrated in Figure 1. There exist two shock fronts due to shock reformation. The old shock front locates at  $\frac{x}{d_{i0}} \approx 96.1$ , while a new one is situated at  $\frac{x}{d_{i0}} \approx 94.5$ . In the ramps of both the old and new shock fronts, the strength of the magnetic field and plasma density increase rapidly. When the upstream particles encounter the ramps, the electrons are magnetized, while the ions can be considered as unmagnetized because their gyro-radii are comparable to the scale of the magnetic field gradient. Therefore, the electrons experience more deceleration than the ions, which generates a charge separation in the shock ramps at a scale smaller than the ion gyro-radius. The existence of an ion-scale electric field at the ramp of quasi-perpendicular shocks has been confirmed by previous shock simulations and observations (Johlander et al., 2023; Scholer et al., 2003; Walker et al., 2004; Wilson et al., 2021; Yang et al., 2009). The ion-scale negative  $E_x$  caused by this charge separation can be observed at the ramps of both the new and the old shock front, which are around  $93.5 < \frac{x}{d_{i0}} < 95.0$  and  $96.0 < \frac{x}{d_{i0}} < 96.3$  as shown in Figure 1a. At the new shock ramp, the negative  $E_x$  has a width of about  $1.5d_{i0}$ . At the old shock ramp, as the compression becomes stronger and the magnetic field gradient becomes larger, the electric field occurs at sub-ion scales (about  $0.2d_{i0}$ ). The electric field at the shock ramps can lead to the electric drift of electrons in the  $y$  direction ( $V_{dye} = -\frac{E_x B_z}{B^2}$ ) (Figure 1b). For convenience, we define the sub-ion scale electric field at the old shock ramp as  $E_{ramp}$ , and focus on the physical processes at this place.

Due to the existence of  $E_{ramp}$ , the electric drift of electrons creates a sub-ion-scale electron velocity shear layer at the old shock ramp, which is unstable to EKHI. In the selected area within the dashed box in Figures 1a and 1b

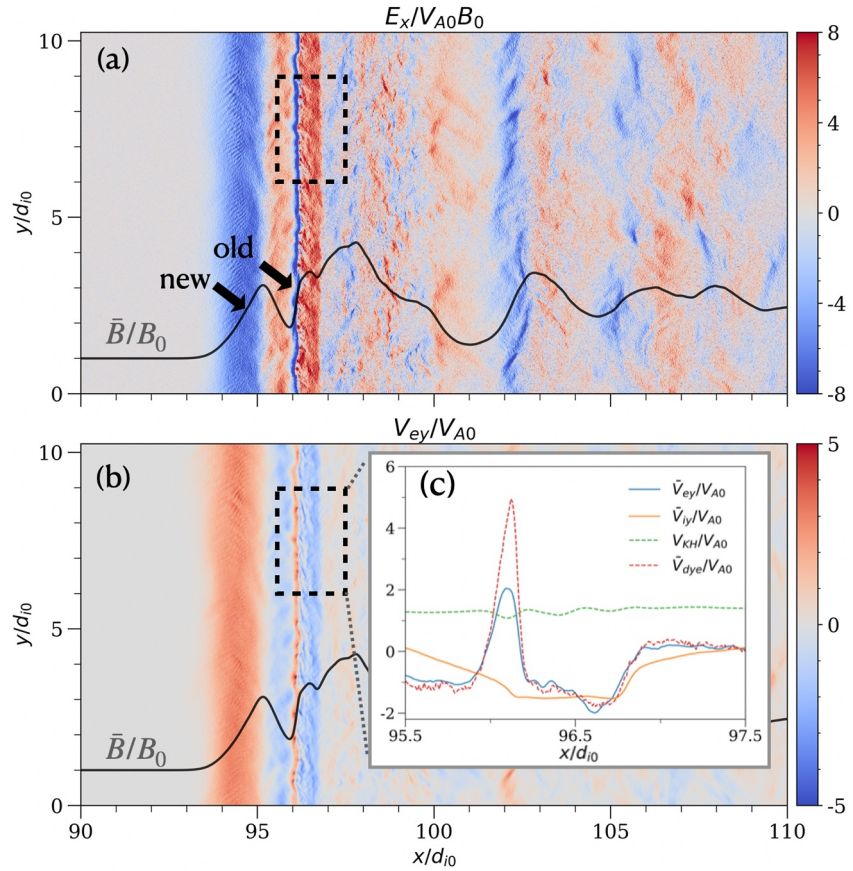


**Figure 1.** The 2D structure of the shock at simulation time  $\Omega_0 t = 16.6$ . (a) The electric field  $E_x$ . (b) The electron flow velocity in the  $y$  direction  $V_{ey}$ . The solid lines in (a, b) represent the magnetic field strength averaged over the  $y$  axis:  $\bar{B} = \sqrt{B_x^2 + B_y^2 + B_z^2}$ . (c) The ion flow velocity, the electron flow velocity, and the electric drift velocity in the  $y$  direction within the dashed box averaged over the  $y$  axis:  $\bar{V}_{iy}$ ,  $\bar{V}_{ey}$ , and  $\bar{V}_{dye}$ . The critical shear velocity  $V_{KH}$  in Equation 2 for EKHI to grow is also plotted. Positions with  $\bar{V}_{ey} < V_{KH}$  are unstable for the shear layer.

( $95.5 \leq \frac{x}{d_{i0}} \leq 97.5$ ;  $6 \leq \frac{y}{d_{i0}} \leq 9$ ), the electron velocity in the  $y$  direction remains close to the electric drift velocity  $V_{dye}$  (Figure 1c) at most positions. At the center of the shear layer ( $x = 96$  to  $96.15d_{i0}$ ),  $\bar{v}_{ey}$  becomes smaller than  $\bar{v}_{dye}$ , which is due to the gradient of electron pressure in the shock ramp causing additional electron diamagnetic drift ( $\mathbf{v}_D = \frac{\nabla p_e \times \mathbf{B}}{en_e B^2}$ , see Figure S1 in Supporting Information S1). The difference in  $V_{ey}$  between the shock ramp and the downstream region is about  $2.5V_{A0}$  (Figure 1c). As  $E_{ramp}$  has a width of about only  $0.2d_{i0}$ , the ion motion is demagnetized, and the ion shear flow is much weaker (Figure 1c). The EKHI has two different modes: the electrostatic (ES) mode (Che, 2024) and the electromagnetic (EM) mode (Che & Zank, 2023). Here, as the electrons are magnetized and the effects of the out-of-plane magnetic field can not be neglected, we consider the EM mode. The shear flow is mainly in the  $y$  direction, therefore the threshold for the excitation of EKHI can be written as (Che & Zank, 2023):

$$|V_{ey1} - V_{ey2}| > \sqrt{\frac{n_{e1} + n_{e2}}{4\pi m_e n_{e1} n_{e2}}} (B_{y1}^2 + B_{y2}^2). \quad (1)$$

where  $V_{ey}$  is the electron flow velocity in the  $y$  direction,  $n_e$  is the electron density, and the subscripts 1 and 2 represent physical quantities at two different positions on the  $x$  axis. Then, we use the subscript “M” to represent the physical quantities at the position where  $V_{ey}$  is maximum ( $\frac{x}{d_{i0}} = 96.1$ ) in the selected area, and the instability criterion is obtained:



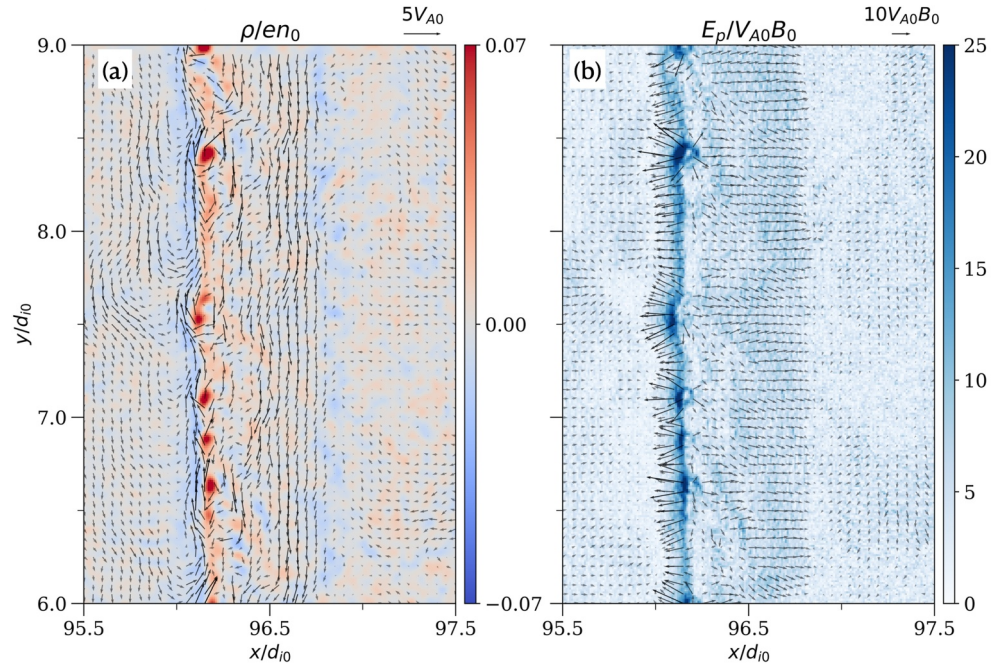


**Figure 2.** Enlarged view of the area within the dashed box in Figure 1 ( $95.5 \leq \frac{x}{d_{i0}} \leq 97.5$ ;  $6 \leq \frac{y}{d_{i0}} \leq 9$ ). (a) The charge density  $\rho = e(n_i - n_e)$ , with the arrows representing the in-plane electron flow velocity. (b) The intensity of the in-plane electric field  $E_p = \sqrt{E_x^2 + E_y^2}$ , with the arrows representing its direction.

$$V_{ey} < V_{eyM} - \sqrt{\frac{n_{eM} + n_e}{4\pi m_e n_{eM} n_e} (B_{yM}^2 + B_y^2)}. \quad (2)$$

We can further define the right-hand side of Equation 2 as  $V_{KH}$ , which is the threshold for the instability. Both the left and right boundaries of the electron shear layer are unstable ( $\bar{V}_{ey} < V_{KH}$ ) to the EKHI (Figure 1c). The growth of the rippled structures of the electron shear layer caused by this instability can also be observed in Movies S1 and S2.

As the EKHI evolves, electron vortices are formed within the electron shear layer, which is shown in Figure 2a. These vortices have a diameter of about  $0.1d_{i0}$  and are distributed apart from each other by about  $0.2$  to  $0.5d_{i0}$ , they move together with the shear flow along  $+y$  direction at a speed of about  $2.6V_{A0}$  (see Movie S3). This suggests that the wavelength of the EKHI is on electron inertial scales ( $2-5d_{e0}$ ), which is consistent with the theory of the EM mode EKHI (Che & Zank, 2023). This wavelength is much larger than the Debye scale, which allows us to rule out the possibility that the observed instability is either the Buneman instability or the ES EKHI. The EKHI can effectively transport the electrons across the shear layer and cause charge separation at sub-ion scales (Lee et al., 2015). Low-density electrons upstream of the shock ramp are transported downstream by the electron vortices, resulting in a decrease in the electron density at the vortex centers. At the same time, because the ions are demagnetized and almost do not react to these small-scale electron vortices, charge separation occurs. Positive charges are cumulated at the centers of the vortices (Figure 2a). As a result, a strong electric field diverging from the vortex centers is formed (Figure 2b). Note that this electric field around the vortices ( $E_{vortex}$ ) has a magnitude of about  $20V_{A0}B_0$ , which is much stronger than  $E_{ramp}$  shown in Figure 1a.

Figure 3b shows the distribution of electron velocity in the direction parallel to the magnetic field within one representative electron vortex at  $96.11 \leq \frac{x}{d_{i0}} \leq 96.23$ ,  $8.28 \leq \frac{y}{d_{i0}} \leq 8.43$ . Notably, a distinct beam component is observed at  $\frac{p_{\parallel}}{m_e V_{A0}} \approx 20$ . We further define those electrons with large parallel momentum,  $\frac{p_{\parallel}}{m_e V_{A0}} > 19$ , as the beam electrons, and their spatial distribution is shown in Figure 3a. These beam electrons are concentrated at the centers of electron vortices. This indicates that the vortices act as a source of producing electron beams at the shock ramp.

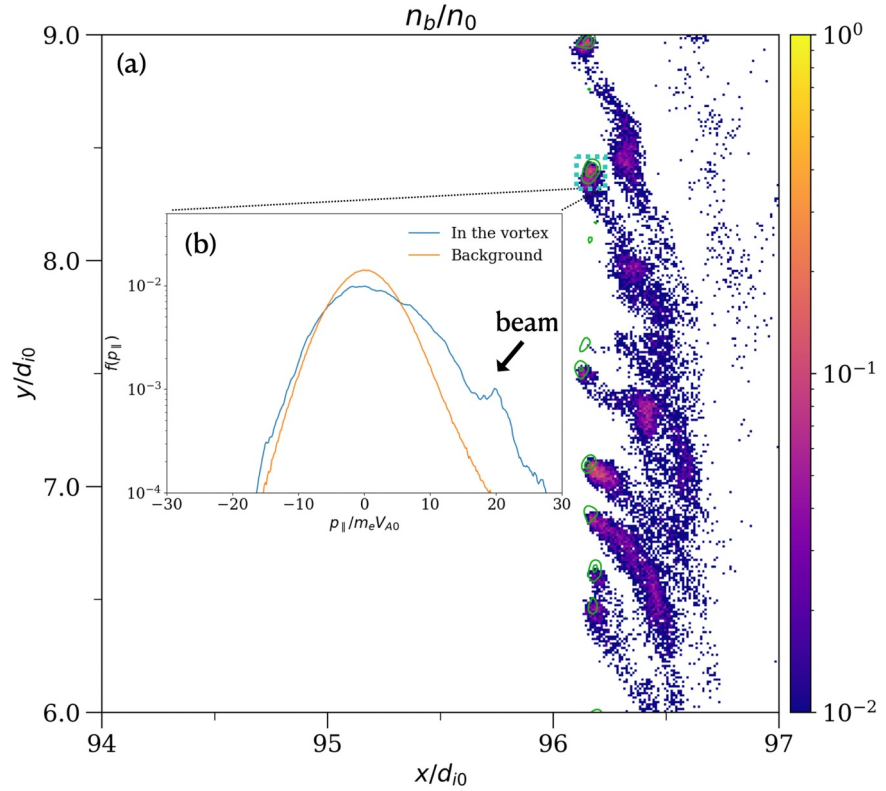


**Figure 3.** (a) The number density of the beam components  $n_b$  (which is defined by electrons with large momentum parallel to the magnetic field:  $\frac{p_{\parallel}}{m_e V_{A0}} > 19$ ). The green lines are the contours of charge density  $\rho$ , which mark out the locations of electron vortices. (b) The blue line represents the normalized parallel momentum distribution for electrons in the vortex marked out by the blue dashed box in (a) ( $96.11 \leq \frac{x}{d_0} \leq 96.23$ ;  $8.28 \leq \frac{y}{d_0} \leq 8.43$ ), and the orange line shows the background electron distribution in  $96.11 \leq \frac{x}{d_0} \leq 96.23$ ,  $0 \leq \frac{y}{d_0} \leq 10.24$  for comparison.

After their formation, these beam electrons leave the vortices and move downstream, resulting in the “tail” distributions downstream of the vortices in Figure 3a.

To comprehend the generation of field-aligned electron beams in the electron vortices, we tracked  $6 \times 10^6$  electrons in our simulation. We can analyze the electron motion by using the guiding center approximation:

$$\mathbf{v}_{\text{guide}} = v_{\parallel} \hat{\mathbf{b}} + \mathbf{v}_{\text{de}} + \mathbf{v}_{\text{cur}} + \mathbf{v}_{\text{gra}}, \quad (3)$$

where  $v_{\parallel}$  is the parallel velocity (the component of the velocity parallel to the magnetic field),  $\mathbf{v}_{\text{de}} = \frac{\mathbf{E} \times \mathbf{B}}{B^2}$  is the electric drift velocity,  $\mathbf{v}_{\text{cur}} = \frac{v_{\parallel}^2 \hat{\mathbf{b}}}{\Omega_{ce}} \times (\hat{\mathbf{b}} \cdot \nabla \hat{\mathbf{b}})$  is the curvature drift velocity, and  $\mathbf{v}_{\text{gra}} = \frac{v_{\parallel}^2 \hat{\mathbf{b}}}{2\Omega_{ce}} \times \frac{\nabla B}{B}$  is the grad-B drift velocity. Figure 4 illustrates the motion of a representative electron accelerated in one of the vortices. At first, this electron enters the shock ramp and drifts in the  $y$  direction due to  $E_{\text{ramp}}$  (Figure 4a). During this period ( $\Omega_{i0} t < 16.3$ ), the trajectory of this electron closely matches the electric drift motion of its guiding center (Figure 4c,  $\Delta x = x(t) - x(t_0) \approx \int_{t_0}^t v_{\text{de},x} dt$ ;  $\Delta y = y(t) - y(t_0) \approx \int_{t_0}^t v_{\text{de},y} dt$ ), and there is no obvious energy increase (Figure 4a). Thereafter, once the electron encounters the electron vortex at ( $\frac{x}{d_0} \approx 96.5$ ;  $\frac{y}{d_0} \approx 7.5$ ), it is trapped around the vortex. During this period ( $\Omega_{i0} t > 16.3$ ), the curvature of the magnetic field in the vortex leads to additional drift of the electron in the  $x$  direction. The electron motion in the  $y$  direction is mainly the electric drift ( $\Delta y \approx \int_{t_0}^t v_{\text{de},y} dt$ ), while the motion in the  $x$  direction consists of both electric drift and curvature drift (Figure 4c,  $\Delta x \approx \int_{t_0}^t v_{\text{de},x} + v_{\text{cur},x} dt$ ). As the trapped electron drifts together with the vortex, it is accelerated rapidly to  $\frac{e}{m_e V_{A0}^2} \approx 400$  (Figures 4b, Movie S4). According to Equation 3, the energy change of the electron can be decomposed into different parts (Northrop, 1963):

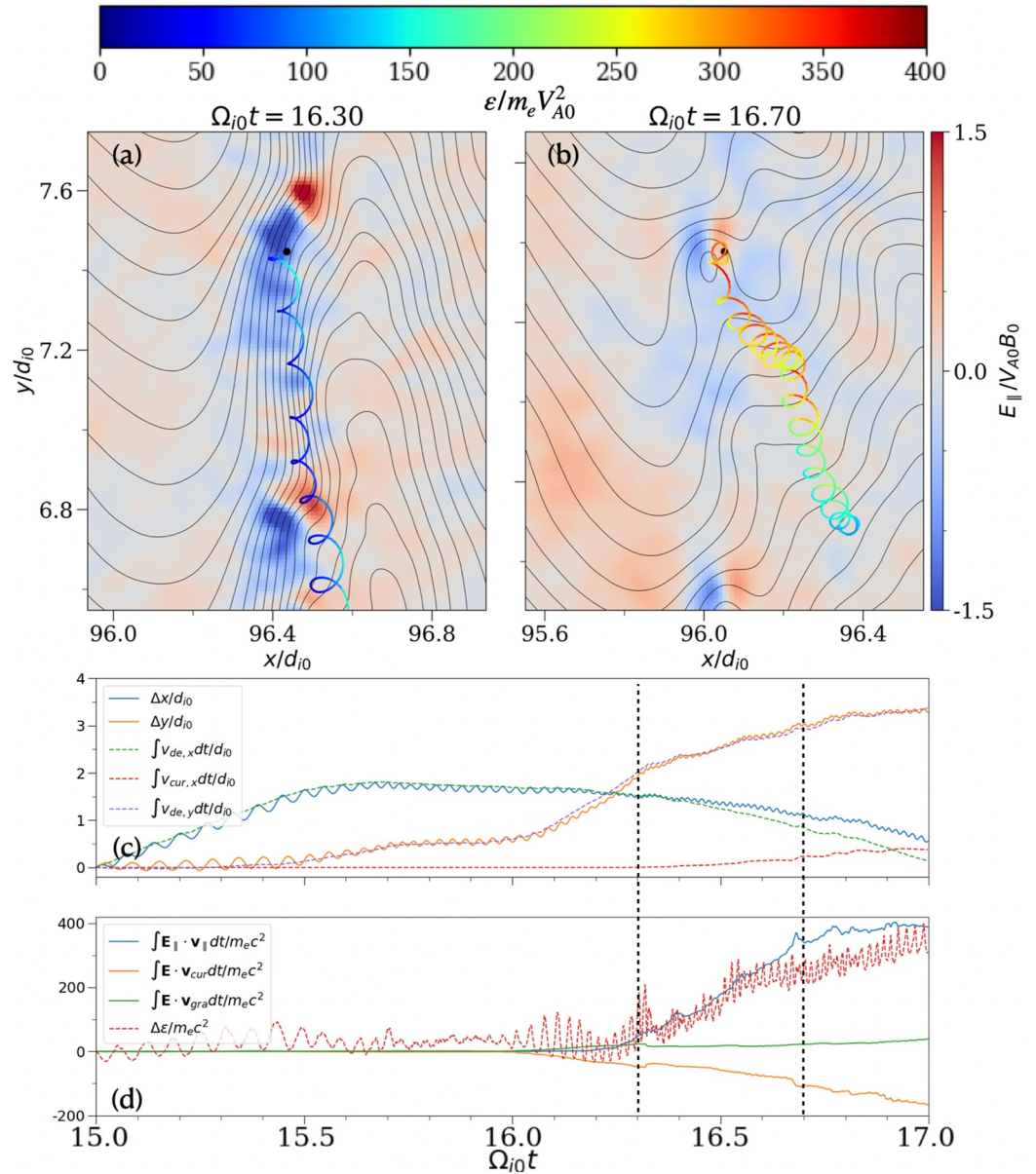


**Figure 4.** (a, b) Trajectory of an electron accelerated in the electron vortex overlaid on the electric field parallel to the magnetic field ( $E_{\parallel}$ ) at  $\Omega_{i0}t = 16.3$  and  $\Omega_{i0}t = 16.7$ . Each bipolar structure of  $E_{\parallel}$  exhibits the position of an electron vortex. The black dot represents the position of the electron. Its trajectory back in  $0.3\Omega_{i0}^{-1}$  is expressed by the colored lines, whose color represents the electron's energy at the corresponding position. (c) The displacement of the selected electron in the  $x$  and  $y$  direction ( $\Delta x = x(t) - x(t_0)$ ), and the displacement of the electron's guiding center obtained from the integrations of the drift velocities in Equation 3. (d) Integrations of the terms in Equation 4, and the energy change of the selected electron ( $\Delta\epsilon = \epsilon(t) - \epsilon(t_0)$ ). Two vertical dashed lines indicate the time points shown in (a, b) ( $\Omega_{i0}t = 16.3$  and  $\Omega_{i0}t = 16.7$ ).

$$\frac{d\epsilon}{dt} \approx \mathbf{v}_{\text{guide}} \cdot \mathbf{E} = E_{\parallel} v_{\parallel} + \mathbf{v}_{\text{gra}} \cdot \mathbf{E} + \mathbf{v}_{\text{cur}} \cdot \mathbf{E} \quad (4)$$

The first term in Equation 4 is the acceleration by the parallel electric field. The second term corresponds to perpendicular heating or cooling due to the grad-B drift. The third term drives parallel acceleration and arises from the first-order Fermi mechanism (Dahlin et al., 2014; Fu et al., 2006; Wang et al., 2017). Figure 4d shows the contribution of these three terms and the energy change of the electron ( $\Delta\epsilon$ ). First,  $\Delta\epsilon$  is consistent with the sum of these three components, which means the guiding center approximation is reasonable here. The contribution of

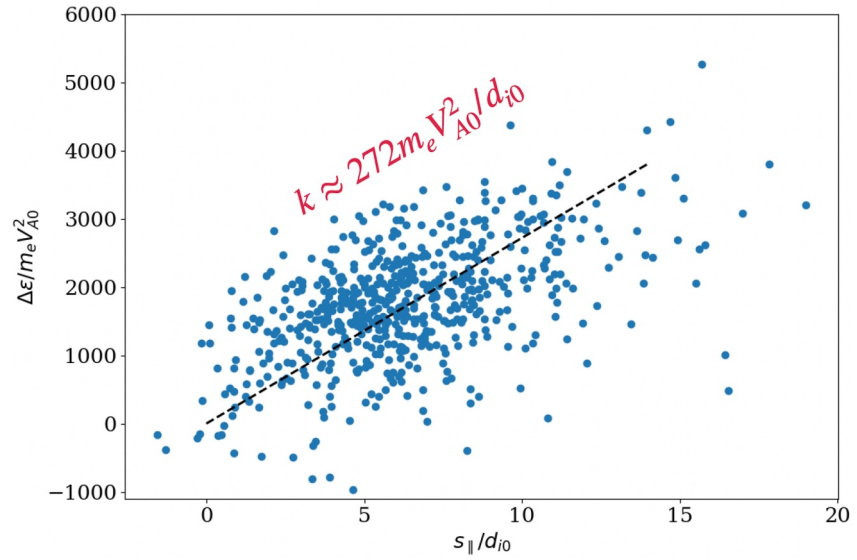


**Figure 5.** Distribution of the energy change of beam electrons ( $\Delta\epsilon$ ) as a function of their displacement in the direction parallel to the magnetic field ( $s_{\parallel} = \int v_{\parallel} dt$ ) during acceleration. The electrons displayed in this figure are accelerated at the electron vortices during  $\Omega_{i0}t = 15.2$  to  $17.0$ .

$v_{\text{gra}} \cdot \mathbf{E}$  can be neglected. The charge separation at the vortex center generates an electric field component parallel to the magnetic field, resulting in a dipole parallel electric field structure around the vortex (Figures 4a and 4b). During the acceleration in the vortex, the work is primarily done by this parallel electric field, while the  $v_{\text{cur}} \cdot \mathbf{E}$  term does negative work. In summary, beam electrons are accelerated by the parallel electric field while drifting together with the electron vortices.

The presented simulation configuration with an out-of-plane component of the magnetic field may limit the possibilities of other kinetic instabilities, which can not be included due to their parallel propagation. This might lead to an overestimation of the electron acceleration in the direction parallel to the magnetic field. We have calculated the displacement of the tracked electron in Figure 4 in the  $z$  direction by integrating its velocity ( $s_z = \int v_z dt$ ). During its acceleration by the parallel component of  $E_{\text{vortex}}$  (from  $\Omega_{i0}t = 16.3$  to  $16.7$ ), the displacement of the tracked electron in the  $z$  direction is about  $6d_{i0}$ . The dominant parallel-propagating wave activity at the ramp of low-Mach-number low-plasma-beta quasi-perpendicular shocks is considered to be the Alfvén ion cyclotron wave (AIC) (McKean et al., 1995, 1996). The wave number  $k$  of AIC at the shock front is found to be around  $0.5d_{i0}^{-1}$  (Hao et al., 2014; McKean et al., 1996), then the corresponding wavelength is  $\lambda_{\text{AIC}} \approx 12.56d_{i0}$ , which is larger than the displacement of the accelerated electron along the  $z$  axis. This means the acceleration process we proposed would not be significantly affected in the three-dimensional configuration. However, the motions of accelerated electrons might be modulated by parallel-propagating waves, which will be an interesting topic for future three-dimensional shock simulations with compatible parameters.

To quantitatively analyze the acceleration efficiency of beam electrons by electron vortices, we identify all the beam electrons ( $\frac{p_{\parallel}}{m_e V_{A0}} > 19$ ) that are accelerated during  $\Omega_{i0}t = 15.2$  to  $17.0$ . The relation between their displacement parallel to the magnetic field ( $s_{\parallel} = \int v_{\parallel} dt$ ) and their energy gain ( $\Delta\epsilon$ ) during the acceleration is shown in Figure 5. A clear correlation can be observed, in which  $\Delta\epsilon$  increases as  $s_{\parallel}$  becomes larger. Since beam electrons are primarily accelerated by the parallel component of  $E_{\text{vortex}}$ , their energy gain in the vortex can be expressed as:

$$\Delta\epsilon \approx -e \int E_{\parallel} v_{\parallel} dt \approx -e \bar{E}_{\parallel} s_{\parallel}, \quad (5)$$

where  $\bar{E}_{\parallel}$  is the average parallel electric field acting on the electrons in the vortex. The slope of the distribution of beam electrons in Figure 5 ( $k \approx \frac{272m_e V_{A0}^2}{d_{i0}}$ ) indicates that  $\bar{E}_{\parallel}$  is approximately  $-2.72V_{A0}B_0$  according to Equation 5.



#### 4. Discussion and Conclusions

We have proposed a novel process to generate electron beams at the ramp of a low-plasma- $\beta$  quasi-perpendicular shock. At the magnetic field gradient of the shock ramp, electrons and ions are separated due to their different gyro-radius. This charge separation generates a sub-ion scale electric field at the shock ramp ( $E_{\text{ramp}}$ ). The electric drift of electrons in  $E_{\text{ramp}}$  then creates a shear flow layer. The shear layer is unstable to EKHI, where electron vortices are formed as the instability develops. The electron vortices transport low-density upstream electrons into the high-density downstream environment, while ions do not respond to these small-scale structures. This causes strong charge separation at the vortex centers. The electric field around the vortices ( $E_{\text{vortex}}$ ) creates a parallel electric field, which directly accelerates thermal electrons. At last, field-aligned electron beams are generated by these vortex-accelerated electrons at the shock ramp. This acceleration mechanism can not only directly accelerate thermal electrons, but also shows comparable efficiency with the traditional SDA mechanism. The overall picture may play an important role in producing electron beams at CME-driven shocks in the solar corona and near-sun solar wind.

In the SDA mechanism, part of the upstream electrons are mirror-reflected by the shock and accelerated by the motional electric field  $\mathbf{E}_{\text{motional}}$ . The resulting average momentum gain of the accelerated electrons is  $\Delta p \sim \frac{2m_e V_{A0} M_A}{\cos \theta_{Bn}}$  (Amano et al., 2022). This means the average energy gain of SDA in our simulation is  $\Delta \epsilon \sim 6000 m_e V_{A0}^2$ , while the average energy gain of the vortex-accelerated electrons is about  $2300 m_e V_{A0}^2$  (Figure 5). However, to enter the SDA process, electrons must be distributed outside the shock's loss cone initially. In low-plasma- $\beta$  environments, thermal electrons can hardly be directly accelerated by SDA. In the process we proposed, thermal electrons are directly accelerated by the parallel component of  $E_{\text{vortex}}$  when they get trapped in the electron vortices, which does not need any prerequisites.

#### Data Availability Statement

The simulation data used to plot the figures in this article can be downloaded from “National Space Science Data Center, National Science and Technology Infrastructure of China” (Guo, 2024).

#### References

- Amano, T., Matsumoto, Y., Bohdan, A., Kobzar, O., Matsukiyo, S., Oka, M., et al. (2022). Nonthermal electron acceleration at collisionless quasi-perpendicular shocks. *Reviews of Modern Plasma Physics*, 6(1), 29. <https://doi.org/10.1007/s41614-022-00093-1>
- Bale, S. D., Balikhin, M. A., Horbury, T. S., Krasnoselskikh, V. V., Kucharek, H., Möbius, E., et al. (2005). Quasi-perpendicular shock structure and processes. *Space Science Reviews*, 118(1–4), 161–203. <https://doi.org/10.1007/s11214-005-3827-0>
- Bale, S. D., Goetz, K., Harvey, P. R., Turin, P., Bonnell, J. W., Dudok de Wit, T., et al. (2016). The FIELDS instrument suite for solar probe plus. *Space Science Reviews*, 204(1–4), 49–82. <https://doi.org/10.1007/s11214-016-0244-5>
- Bale, S. D., Reiner, M. J., Bougeret, J.-L., Kaiser, M. L., Krucker, S., Larson, D. E., & Lin, R. P. (1999). The source region of an interplanetary type II radio burst. *Geophysical Research Letters*, 26(11), 1573–1576. <https://doi.org/10.1029/1999GL900293>
- Balogh, A., & Treumann, R. A. (2013). *Physics of collisionless shocks: Space plasma shock waves*. Springer. <https://doi.org/10.1007/978-1-4614-6099-2>
- Bell, A. R. (1978). The acceleration of cosmic rays in shock fronts—I. *Monthly Notices of the Royal Astronomical Society*, 182(2), 147–156. <https://doi.org/10.1093/mnras/182.2.147>
- Biskamp, D., & Welter, H. (1972). Ion heating in high-Mach-number, oblique, collisionless shock waves. *Physical Review Letters*, 28(7), 410–413. <https://doi.org/10.1103/PhysRevLett.28.410>
- Burgess, D., Lucek, E. A., Scholer, M., Bale, S. D., Balikhin, M. A., Balogh, A., et al. (2005). Quasi-parallel shock structure and processes. *Space Science Reviews*, 118(1–4), 205–222. <https://doi.org/10.1007/s11214-005-3832-3>
- Che, H. (2024). Plasma compressibility and the generation of electrostatic electron Kelvin–Helmholtz instability. *Physics of Plasmas*, 31(7), 072102. <https://doi.org/10.1063/5.0208134>
- Che, H., & Zank, G. P. (2023). Electromagnetic electron Kelvin–Helmholtz instability. *Physics of Plasmas*, 30(6), 062110. <https://doi.org/10.1063/5.0150895>
- Dahlin, J. T., Drake, J. F., & Swisdak, M. (2014). The mechanisms of electron heating and acceleration during magnetic reconnection. *Physics of Plasmas*, 21(9). <https://doi.org/10.1063/1.4894484>
- Derouillat, J., Beck, A., Pérez, F., Vinci, T., Chiaramello, M., Grassi, A., et al. (2018). Smilei: A collaborative, open-source, multi-purpose particle-in-cell code for plasma simulation. *Computer Physics Communications*, 222, 351–373. <https://doi.org/10.1016/j.cpc.2017.09.024>
- Drury, L. O. C. (1983). An introduction to the theory of diffusive shock acceleration of energetic particles in tenuous plasmas. *Reports on Progress in Physics*, 46(8), 973–1027. <https://doi.org/10.1088/0034-4885/46/8/002>
- Fu, X. R., Lu, Q. M., & Wang, S. (2006). The process of electron acceleration during collisionless magnetic reconnection. *Physics of Plasmas*, 13(1), 012309. <https://doi.org/10.1063/1.2164808>
- Guo, A. (2024). Data for “electron beams generated by the electron Kelvin–Helmholtz instability at a quasi-perpendicular shock” [Dataset]. *Science Data Bank*. <https://doi.org/10.57760/sciencedb.13633>
- Gurnett, D. A., Neubauer, F. M., & Schwenn, R. (1979). Plasma wave turbulence associated with an interplanetary shock. *Journal of Geophysical Research*, 84(A2), 541–552. <https://doi.org/10.1029/JA084iA02p00541>

#### Acknowledgments

This work was supported by the National Natural Science Foundation of China (NSFC) Grants 42230201, 42188101, 42150105 and 42274210, National Key Research and Development Program of China (Nos. 2022YFA1604600 and 2021YFA0718600), and the Strategic Priority Research Program of Chinese Academy of Sciences, Grants XDB 41000000 and XDB0560000. Z. W. Yang is supported by the pre-research Project on Civil Aerospace Technologies (D010202).



- Hao, Y. F., Lu, Q. M., Gao, X. L., Huang, C., Lu, S., Shan, L. C., & Wang, S. (2014). He<sup>2+</sup> dynamics and ion cyclotron waves in the downstream of quasi-perpendicular shocks: 2-D hybrid simulations. *Journal of Geophysical Research: Space Physics*, *119*(5), 3225–3236. <https://doi.org/10.1002/2013JA019717>
- Hellinger, P., Trávníček, P., & Matsumoto, H. (2002). Reformation of perpendicular shocks: Hybrid simulations. *Geophysical Research Letters*, *29*(24), 2234. <https://doi.org/10.1029/2002GL015915>
- Holman, G. D., & Pesses, M. E. (1983). Solar type II radio emission and the shock drift acceleration of electrons. *The Astrophysical Journal*, *267*, 837. <https://doi.org/10.1086/160918>
- Jebaraj, I. C., Kouloumvakos, A., Magdalenic, J., Rouillard, A. P., Mann, G., Krupar, V., & Poedts, S. (2021). Generation of interplanetary type II radio emission. *Astronomy & Astrophysics*, *654*, A64. <https://doi.org/10.1051/0004-6361/202141695>
- Johlander, A., Khotyaintsev, Y. V., Dimmock, A. P., Graham, D. B., & Lalti, A. (2023). Electron heating scales in collisionless shocks measured by MMS. *Geophysical Research Letters*, *50*(5). <https://doi.org/10.1029/2022GL100400>
- Lee, S.-Y., Lee, E., Kim, K.-H., Lee, D.-H., Seon, J., & Jin, H. (2015). Electron Debye scale Kelvin-Helmholtz instability: Electrostatic particle-in-cell simulations. *Physics of Plasmas*, *22*(12), 122113. <https://doi.org/10.1063/1.4938201>
- Lembège, B., & Dawson, J. M. (1987). Self-consistent study of a perpendicular collisionless and nonresistive shock. *Physics of Fluids*, *30*(6), 1767–1788. <https://doi.org/10.1063/1.866191>
- Lembège, B., & Savoini, P. (2002). Formation of reflected electron bursts by the nonstationarity and nonuniformity of a collisionless shock front. *Journal of Geophysical Research*, *107*, A3. <https://doi.org/10.1029/2001JA900128>
- Lindberg, M., Vaivads, A., Raptis, S., & Karlsson, T. (2023). MMS observation of two-step electron acceleration at Earth's Bow shock. *Geophysical Research Letters*, *50*(16), e2023GL104714. <https://doi.org/10.1029/2023GL104714>
- Maguire, C. A., Carley, E. P., McCauley, J., & Gallagher, P. T. (2020). Evolution of the Alfvén Mach number associated with a coronal mass ejection shock. *Astronomy & Astrophysics*, *633*, A56. <https://doi.org/10.1051/0004-6361/201936449>
- Maloney, S. A., & Gallagher, P. T. (2011). STEREO direct imaging of a coronal mass ejection-driven shock to 0.5 AU. *The Astrophysical Journal Letters*, *736*(1), L5. <https://doi.org/10.1088/2041-8205/736/1/L5>
- Matsukiyo, S., & Scholer, M. (2012). Dynamics of energetic electrons in nonstationary quasi-perpendicular shocks. *Journal of Geophysical Research*, *117*(A11), A11105. <https://doi.org/10.1029/2012JA017986>
- McKean, M. E., Omid, N., & Krauss-Varban, D. (1995). Wave and ion evolution downstream of quasi-perpendicular bow shocks. *Journal of Geophysical Research*, *100*(A3), 3427–3437. <https://doi.org/10.1029/94JA02529>
- McKean, M. E., Omid, N., & Krauss-Varban, D. (1996). Magnetosheath dynamics downstream of low Mach number shocks. *Journal of Geophysical Research*, *101*, 20013. <https://doi.org/10.1029/96JA01461>
- Melrose, D. B. (1980). The emission mechanisms for solar radio bursts. *Space Science Reviews*, *26*(1), 3–38. <https://doi.org/10.1007/BF00212597>
- Melrose, D. B. (2017). Coherent emission mechanisms in astrophysical plasmas. *Reviews of Modern Plasma Physics*, *1*, 5. <https://doi.org/10.1007/s41614-017-0007-0>
- Morosan, D. E., Carley, E. P., Hayes, L. A., Murray, S. A., Zucca, P., Fallows, R. A., et al. (2019). Multiple regions of shock-accelerated particles during a solar coronal mass ejection. *Nature Astronomy*, *3*(5), 452–461. <https://doi.org/10.1038/s41550-019-0689-z>
- Northrop, T. G. (1963). Adiabatic charged-particle motion. *Reviews of Geophysics*, *1*(3), 283–304. <https://doi.org/10.1029/RG001i003p00283>
- Pulupa, M. P., Bale, S. D., & Kasper, J. C. (2010). Langmuir waves upstream of interplanetary shocks: Dependence on shock and plasma parameters. *Journal of Geophysical Research*, *115*(A4), A04106. <https://doi.org/10.1029/2009JA014680>
- Scholer, M., Shinohara, I., & Matsukiyo, S. (2003). Quasi-perpendicular shocks: Length scale of the cross-shock potential, shock reformation, and implication for shock surfing. *Journal of Geophysical Research*, *108*(A1), 1014. <https://doi.org/10.1029/2002JA009515>
- Shen, F., Shen, C., Xu, M., Liu, Y., Feng, X., & Wang, Y. (2022). Propagation characteristics of coronal mass ejections (CMEs) in the corona and interplanetary space. *Reviews of Modern Plasma Physics*, *6*, 1. <https://doi.org/10.1007/s41614-022-00069-1>
- Stone, R. G., & Tsurutani, B. T. (1985). Collisionless shocks in the heliosphere: A tutorial review. In *American Geophysical Union Geophysical Monograph Series* (Vol. 34). American Geophysical Union. <https://doi.org/10.1029/GM034>
- Tsurutani, B. T., & Stone, R. G. (1985). Collisionless shocks in the heliosphere: Reviews of current research. In *American Geophysical Union Geophysical Monograph Series* (Vol. 35). American Geophysical Union. <https://doi.org/10.1029/GM035>
- Walker, S. N., Alleyne, H. S., Balikhin, M. A., André, M., & Horbury, T. S. (2004). Electric field scales at quasi-perpendicular shocks. *Annales Geophysicae*, *22*(7), 2291–2300. <https://doi.org/10.5194/angeo-22-2291-2004>
- Wang, H. Y., Lu, Q. M., Huang, C., & Wang, S. (2017). Electron acceleration in a secondary magnetic island formed during magnetic reconnection with a guide field. *Physics of Plasmas*, *24*(5), 052113. <https://doi.org/10.1063/1.4982813>
- Williams, J. D., Chen, L.-J., Kurth, W. S., Gurnett, D. A., Dougherty, M. K., & Rymer, A. M. (2005). Electrostatic solitary structures associated with the November 10, 2003, interplanetary shock at 8.7 AU. *Geophysical Research Letters*, *32*(17), L17103. <https://doi.org/10.1029/2005GL023079>
- Wilson, L. B., Chen, L.-J., & Roytershteyn, V. (2021). The discrepancy between simulation and observation of electric fields in collisionless shocks. *Frontiers in Astronomy and Space Sciences*, *7*. <https://doi.org/10.3389/fspas.2020.592634>
- Wilson, L. B., Sibek, D. G., Turner, D. L., Osmane, A., Caprioli, D., & Angelopoulos, V. (2016). Relativistic electrons produced by foreshock disturbances observed upstream of Earth's Bow Shock. *Physical Review Letters*, *117*(21), 215101. <https://doi.org/10.1103/PhysRevLett.117.215101>
- Wu, C. S. (1984). A fast Fermi process: Energetic electrons accelerated by a nearly perpendicular bow shock. *Journal of Geophysical Research*, *89*(A10), 8857–8862. <https://doi.org/10.1029/JA089iA10p08857>
- Yang, Z. W., Liu, Y. D., Johlander, A., Parks, G. K., Lavraud, B., Lee, E., et al. (2020). MMS direct observations of kinetic-scale shock self-reformation. *The Astrophysical Journal Letters*, *901*(1), L6. <https://doi.org/10.3847/2041-8213/abb3ff>
- Yang, Z. W., Lu, Q. M., & Wang, S. (2009). The evolution of the electric field at a nonstationary perpendicular shock. *Physics of Plasmas*, *16*(12), 124502. <https://doi.org/10.1063/1.3275788>
- Zhang, Y., Davies, J. R., Heuer, P. V., Davies, J. R., Schaeffer, D. B., Wen, H., et al. (2024). Kinetic study of shock formation and particle acceleration in laser-driven quasi-parallel magnetized collisionless shocks. *Physics of Plasmas*, *31*(8), 082303. <https://doi.org/10.1063/5.0210050>
- Zhang, Y., Davies, J. R., Heuer, P. V., & Ren, C. (2021). Kinetic simulation study of magnetized collisionless shock formation on a terawatt laser system. *Physics of Plasmas*, *28*(7), 072111. <https://doi.org/10.1063/5.0050894>